Sensors and Actuators B 221 (2015) 1499–1507

Contents lists available at ScienceDirect

Sensors and Actuators B: Chemical

journal homepage: www.elsevier.com/locate/snb

Excellent gas detection of ZnO nanofibers by loading with reduced graphene oxide nanosheets

Zain Ul Abideen [a], Akash Katoch [a], Jae-Hun Kim [a], Yong Jung Kwon [b], Hyoun Woo Kim [b,*], Sang Sub Kim [a,**]

[a] Department of Materials Science and Engineering, Inha University, Incheon 402-751, Republic of Korea
[b] Division of Materials Science and Engineering, Hanyang University, Seoul 133-791, Republic of Korea

ARTICLE INFO

Article history:
Received 21 May 2015
Received in revised form 28 July 2015
Accepted 31 July 2015
Available online 3 August 2015

Keywords:
Reduced graphene oxide
ZnO nanofiber
Electrospinning
Chemical sensor

ABSTRACT

We have fabricated sensors with reduced graphene oxide (RGO) nanosheets (NSs)-loaded ZnO nanofibers (NFs) via an electrospinning method. The RGO NSs-loaded ZnO NFs were comprised of nanograins with an average diameter of 20 nm. Transmission electron microscopy and X-ray diffraction both revealed the presence of RGO NSs in the ZnO NFs. The sensing properties of RGO NSs-loaded ZnO NFs were examined after exposure to various gases, including O_2, SO_2, NO_2, CO, C_6H_6, and C_2H_5OH. The sensor responses showed a bell-shaped behavior with respect to the weight ratio of RGO NSs. It is remarkable that our sensors exhibited significantly higher responses than pure ZnO NFs. We propose a novel hybrid sensing mechanism for the drastic improvement in the sensing behavior that is caused by loading RGO NSs into ZnO NFs. This hybrid sensing mechanism combines the resistance modulation of ZnO/ZnO homointerfaces and RGO-NSs/ZnO heterointerfaces in addition to the radial modulation of the surface depletion layer of ZnO NFs. In the heterointerfaces, the creation of local heterojunctions plays a significant role in raising the sensitivity of RGO-loaded ZnO NFs.

1. Introduction

The sensing ability of materials can be greatly increased by reducing their size down to the nanometer scale, presumably through the preparation of nanodots, nanowires, nanofibers, and nanowebs [1]. However, nanofibers (NFs), which are one-dimensional nanostructures comprised of many nanograins, have been identified as the most promising structure for the successful detection of analytes (even when the concentration is as low as ppb) among the various types of nanostructures [2]. The extraordinary sensing properties of NFs are primarily ascribed to their large surface to volume ratio as compared to other nanostructures. Due to the fact that they contain many small grains, NFs possess large grain boundary areas. Consequently, a larger amount of analytes can diffuse along the boundaries, resulting in enhanced sensitivity. Many synthesis procedures for NFs have been investigated over the last few decades, but electrospun NFs are dominant in chemical sensor applications because the processing parameters and the characteristics (e.g., morphology, diameter, aspect ratio, nature of the NFs, etc.) of the NFs can be easily controlled; these variables heavily influence the chemical sensing abilities. In addition, the electrospinning method is incredibly effective for low-cost mass production with the minimal usage of materials, which makes it the most suitable method for industrial applications on the commercial scale. For these reasons, electrospun NFs have been employed in a diverse range of sensing materials [3–14]. Possessing a wide bandgap (3.37 eV) with a large exciton energy (60 meV) [15], ZnO NFs-based semiconductors are one of the most promising sensing materials and have been extensively studied for the past several years [16–18]. However, despite their inherent advantageous characteristics, there is still room for improvement. Because ZnO-based sensors are usually good for high temperature environments, they oftentimes require more power, which affects their long term stability. Further enhancement of their sensing performance is strongly required.

In order to efficiently improve the sensitivity of nanostructured gas sensors, researchers are currently pursuing synergistic effects between different nanomaterials. Recently, the use of dopants (including Au [19], Ag [20], Pt [21], and Pd [22]) and the creation of local *p*–*n* heterojunctions in *n*-type ZnO (by mixing with

* Corresponding author at: 222 Wangsimni-ro, Seongdong-gu, Seoul 133-791, Republic of Korea.
** Corresponding author at: 100 Inha-ro, Nam-gu, Incheon 402-751, Republic of Korea.
E-mail addresses: hyounwoo@hanyang.ac.kr (H.W. Kim), sangsub@inha.ac.kr (S.S. Kim).

http://dx.doi.org/10.1016/j.snb.2015.07.120
0925-4005/

p-type semiconductors such as $BaTiO_3$–CuO–La_2O_3 [23], CuO [24], and graphene [25]) have significantly improved the sensing performance of ZnO-based gas sensors. Additionally, chemically derived graphene is expected to be a highly sensitive chemical sensor because of its very high electron mobility [26,27]. Since it is an exceptionally low-noise material, graphene sensors should be able to detect individual gas molecules and are expected to exhibit an excellent sensing behavior [28]. However, pure graphene faces difficulties in being employed as a practical sensor because its adsorption of gas molecules is inefficient. In this regard, reduced graphene oxide (RGO), which is graphene decorated with oxygen functional groups that provide an increased amount of adsorption sites, is more beneficial for improving sensitivity [29]. A recent study found that highly dispersed ZnO nanoparticles on a graphene surface showed higher sensitivity toward 1000 ppm of acetylene gas [30]. However, for practical applications, more efficient sensors that can effectively detect very small traces of gases are required. Furthermore, properly optimizing the quantity of the RGO is crucial in order to obtain the best sensing performance for small traces of gases that also avoids overloading of the dopant and minimizes the cost. To the best of the authors' knowledge, no attempts have been reported regarding the creation of local heterojunctions in *n*-ZnO NFs with RGO.

Herein, we investigated the sensing properties of *n*-ZnO NFs doped with RGO nanosheets (NSs). Our synthesis utilizes a very simple and cost-effective electrospinning method. The present RGO-loaded ZnO NFs contain several characteristics that are favorable for gas sensors. Not only do these sensors utilize the largest grain boundary area provided by the electrospun NF structure, but they also consist of sensing materials (i.e., ZnO and RGO) with inherently advantageous characteristics. Furthermore, these sensors create local *p*–*n* heterojunctions at the heterointerfaces of ZnO/RGO, achieving the best sensing performance at the optimal amount of RGO for the detection of trace amounts (1, 2, and 5 ppm) of different oxidizing and reducing gases. Detailed characterization of RGO-loaded ZnO NFs is carried out to understand the interactions between RGO NSs and ZnO nanograins. The sensing characteristics are examined as a function of the concentration of RGO NSs. Experimental results indicate that the addition of RGO and the creation of local *p*–*n* heterojunctions greatly improve the sensing characteristics of the ZnO NFs. This is a promising method to fabricate practical sensors with high sensing capabilities. In this regard, we explain the novel hybrid sensing mechanism of these composite NFs, which enables their exceptionally high response to all gases. The presented synthesis procedure, which is both simple and cost-effective, is beneficial for the practical fabrication of these detectors.

2. Experimental

2.1. Materials

Zinc acetate ($(CH_3CO_2)_2Zn$, Sigma Aldrich Corp.), reduced graphene oxide, and polyvinyl alcohol (PVA, MW 80,000, Sigma Aldrich Corp.) were used as-received without any further processing or refining. The preparation process of RGO solution is described in detail in a previous report [31].

2.2. Synthesis of NFs and sensing device fabrication

The procedure to synthesize RGO-loaded ZnO NFs is as follows: first an aqueous solution of PVA (10 wt%) was prepared, in which PVA was dissolved in distilled water. After 4 h of continuous stirring at 65–70 °C, the zinc acetate and RGO solution was added to the PVA solution, subsequently being stirred for an additional 6 h at 70 °C. Since TEM investigation of RGO-loaded ZnO NFs does not clearly show the individual image of RGO nanosheests, we estimated the sizes of RGO nanosheets in source materials, from many TEM images. The average size was measured to be about 75 nm, which is smaller than the diameter of ZnO NFs.

Next, this viscous solution was used to produce RGO-loaded ZnO NFs by a conventional electrospinning method; the prepared viscous solution was loaded into a syringe equipped with a 21-guage stainless steel needle with an inner diameter of 0.51 mm. Applied voltage, feed rate, and distance between the collector and the needle tip were set to 15 kV, 0.03 mL/h, and 20 cm, respectively. The voltage was applied to the needle tip, whereas the metal collector was grounded. NFs were deposited onto SiO_2 substrates, with a uniform distribution, as described in our previous reports [15,32] and shown in Fig. 1a. All of the electrospinning experiments were done at room temperature. Calcination of the NFs was carried out in air for 5 h at 500 °C with a heating rate of 0.5 °C/min, to remove the polymer solvents. In total, six sensor devices were fabricated to investigate ZnO NFs containing different quantities of RGO NSs (0.04, 0.11, 0.17, 0.44, 0.77, and 1.04 wt%). Since RGO is known to be stable at temperatures in the range of −10 to 800 °C [33,34], the RGO NS will not be decomposed during the calcination process at 500 °C. Subsequently, for gas sensing measurements, Ti (thickness: ∼50 nm) and Pt (thickness: ∼200 nm) were deposited on the substrates via magnetron sputtering using interdigitated electrodes.

2.3. Characterization and sensing measurements

The microstructural and morphological characteristics of RGO-loaded ZnO NFs were investigated by field-emission scanning electron microscopy (FE-SEM, Hitachi S-4200) and transmission electron microscopy (TEM, Phillips CM-200). The structural phase analysis was carried out using X-ray diffraction (XRD, Phillips X'pert MRD). For SEM, the samples were cleaned by several steps, including ultrasonic cleaning, blow-drying, and drying using oven or hot plate. They were sputter-coated with Pt layer, in order to eliminate the charge effect. For TEM, the samples were dispersed in acetone ultrasonically. Subsequently, drops of the suspension were located on the amorphous carbon films supported on copper grids. The sample-comprising grids were dried in air. Raman spectra were acquired at room temperature with a Raman microscope (LabRam HR800 UV; Horiba Jobin-Yvon, France) at Korea Basic Science Institute (KBSI). The excitation light source was a diode laser with a wavelength of 514 nm. The laser power incident on the sample surface was 10% of 10 mW. The Raman spectrum of RGO-loaded ZnO NFs is shown in Supplementary Material (Fig. S1). The D and G peaks of graphite, being originated from surface RGOs, were observed, in addition to ZnO-related ones.

In order to fabricate the sensor device, we have sputter-deposited Pt (∼200 nm) and Ti (∼50 nm) sequentially, on the specimens by means of using an interdigital electrode mask. The *I*–*V* test showed pseudo-ohmic characteristics (Fig. S2). The sensing performance of RGO-loaded ZnO NFs was investigated for common oxidizing (NO_2, SO_2, and O_2) and reducing (CO, C_6H_6 (benzene), and C_2H_5OH (ethanol)) gases using a custom-made gas-sensing system. The gas sensing measurements were carried out at three different temperatures (300 °C, 350 °C, and 400 °C), which were optimized in our previous reports [32,35]. The gas concentration was controlled using accurate mass flow controllers. For oxidizing gases, the gas response was calculated by R_g/R_a, where R_g is the impedance of the sensor in the applied target gas and R_a is the resistance in the air or in the absence of the target gas. For reducing gases, the gas response was determined to be R_a/R_g.

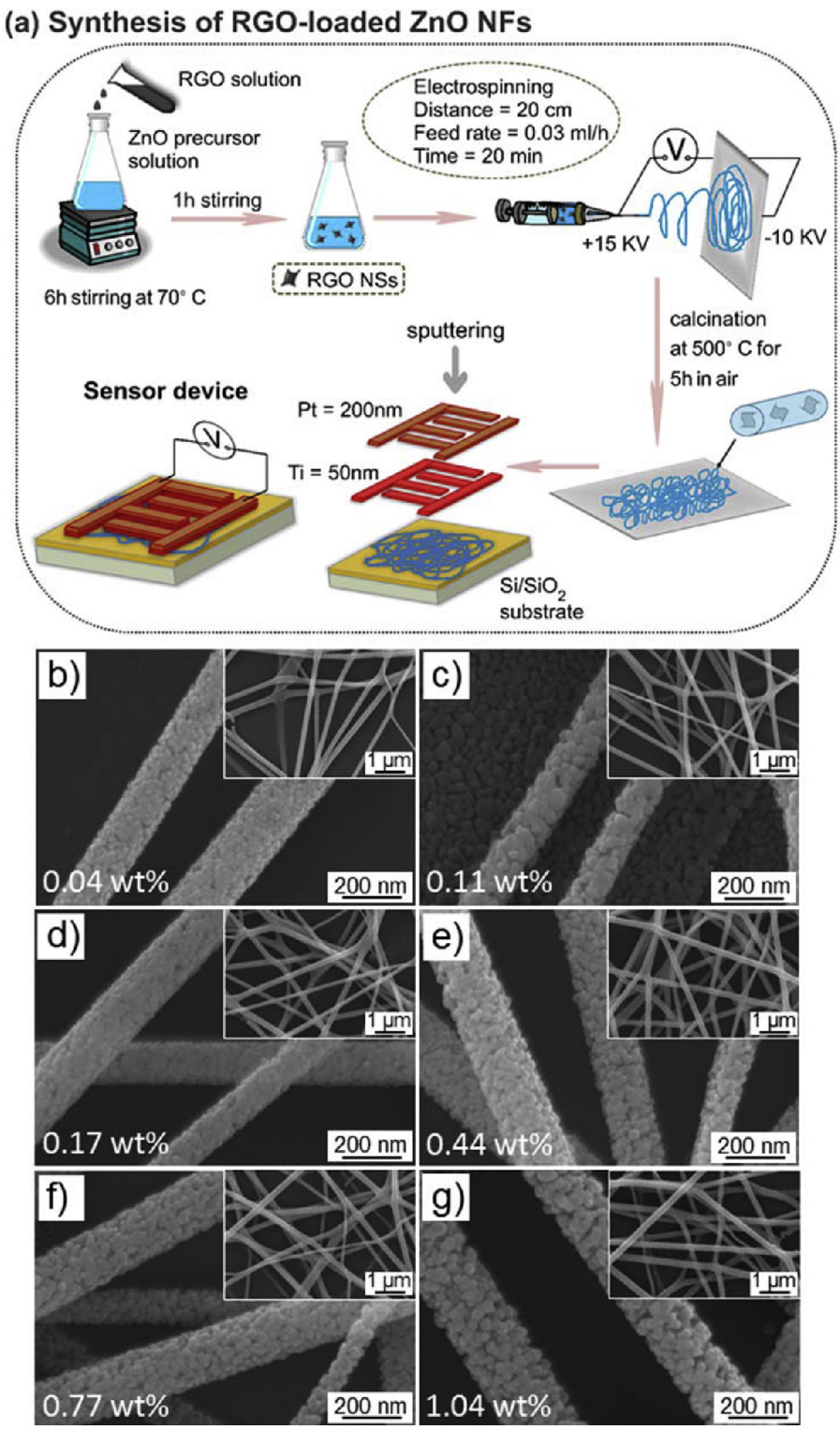

Fig. 1. (a) Schematic illustration of the synthesis of RGO-loaded ZnO nanofibers via electrospinning method. SEM images of calcined RGO-loaded ZnO NFs with a weight ratio of (b) 0.04, (c) 0.11, (d) 0.17, (e) 0.44, (f) 0.77, (g) 1.04.

3. Results and discussion

The microstructures of the synthesized RGO-loaded ZnO NFs are shown in Fig. 1b–g. The average diameter of the calcined NFs is measured to be about 150 nm. Because the sensing properties of oxide-based semiconductor gas sensors are greatly affected by the size of their nanograins [2], SEM images of RGO-loaded ZnO NFs were taken. These images clearly exhibit the existence of nanograins. Fig. 1b–g reveals that the size of the nanograins and/or the diameter of the NFs were not influenced as the amount of RGO NSs was changed. The upper-right insets reveal that the NFs are uniformly distributed on the substrates.

In order to investigate the configuration of RGO NSs and their interactions with ZnO nanograins, we carried out a TEM analysis.

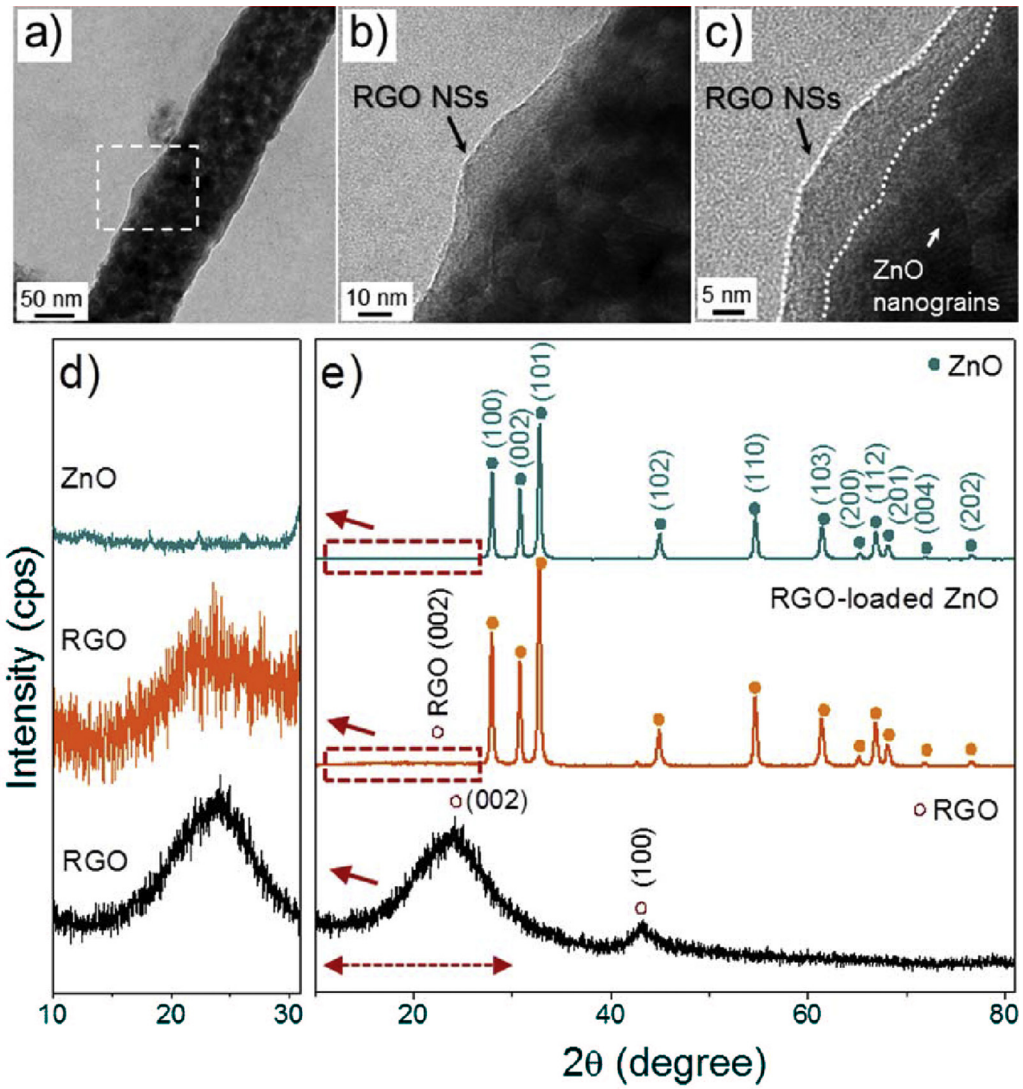

Fig. 2. TEM images showing microstructures of RGO-loaded ZnO NFs. (a) and (b) low magnification, (c) high magnification and (d)–(e) XRD patterns of ZnO NFs, RGO-loaded ZnO NFs and RGO NSs.

Fig. 2a shows a low-magnification TEM image of an RGO-loaded ZnO NF. Fig. 2b is a magnified TEM image that shows an enlarged image of the dotted square in Fig. 2a. In Fig. 2c, the RGO NS can be clearly observed. Also, the presence of nanograins in the TEM images indicates the polycrystalline nature of the ZnO. RGO NSs have been attached to the boundaries of the nanograins, likely creating local heterojunctions with the *n*-type ZnO nanograins. The phase analysis of the synthesized NFs was performed by XRD and supports the presence of RGO NSs in ZnO NFs, as shown in Fig. 2d and e. Fig. 2e shows the representative XRD patterns of monolithic ZnO NFs, RGO-loaded ZnO NFs, and pure RGO NSs, respectively. All of the peaks of RGO-loaded ZnO NFs agree well with those of monolithic ZnO NFs (JCPDS Card No. 891397). However, a broad diffraction peak (d-spacing 3.7 Å at $2\theta = 24.0^\circ$) of RGO NSs was also observed in RGO-loaded ZnO NFs, as clearly depicted in Fig. 2d. This broad diffraction peak of RGO is very close to the typical (002) diffraction peak of graphite (d-spacing 3.35 Å at $2\theta = 26.6^\circ$) [26,36]. From these results, TEM and XRD analyses both confirm the presence of RGO NSs in RGO-loaded ZnO NFs.

The sensing properties of these RGO-loaded ZnO NFs were evaluated by exposing them to different oxidizing (NO_2, SO_2, and O_2) and reducing (CO, C_6H_6, and C_2H_5OH) gases between 300 and 400 °C. The concentrations of the gases were set to 1, 2, and 5 ppm. Fig. 3a summarizes the sensor responses as the weight percent of the RGO was varied between 0 and 1.04 wt%. The NO_2 concentration was set to 5 ppm and the sensing temperature ranged from 300 to 400 °C. The typical dynamic sensing curves for all of the sensors to NO_2 gas at 400 °C are shown in Supplementary material (Fig. S3). Each sensor clearly showed an increase in resistance with the introduction of NO_2 gas. Upon the removal or stoppage of the gas, the sensors again showed a decrease in their resistivity. This trend of changing resistance can be defined in terms of the framework of *n*-type semiconductors, in which the major charge carriers are electrons. NO_2 gas molecules adsorb onto the surfaces of the NFs, diffuse and take electrons from the NFs, and then create electron-depleted regions, eventually leading to the decrease in the conductivity of the NFs. Likewise, emission of electrons occurs when the NO_2 gas is removed. However, the transfer of electrons and the formation of anions (here NO_x^- or oxygen anions in the presence of oxygen) on the surface of the sensing material are significantly dependent on the temperature and sensing material. All sensors containing RGO NSs showed a higher response than pure ZnO NFs at all temperatures. It is noteworthy that the best response was achieved at 400 °C. Fig. 3b shows the variation of sensor responses as the weight percent of the RGO was varied between 0 and 1.04 wt% at an NO_2 concentration and temperature of 5 ppm and 400 °C, respectively.

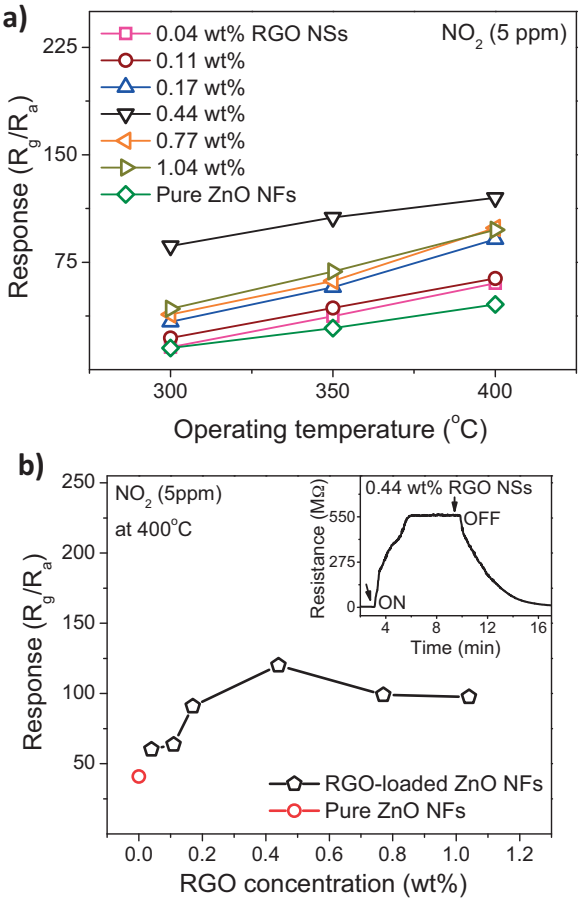

Fig. 3. (a) Response of all sensors to 5 ppm NO_2 gas as a function of temperature and (b) response of all sensors to 5 ppm NO_2 gas as a function of RGO concentration (wt%) at 400 °C.

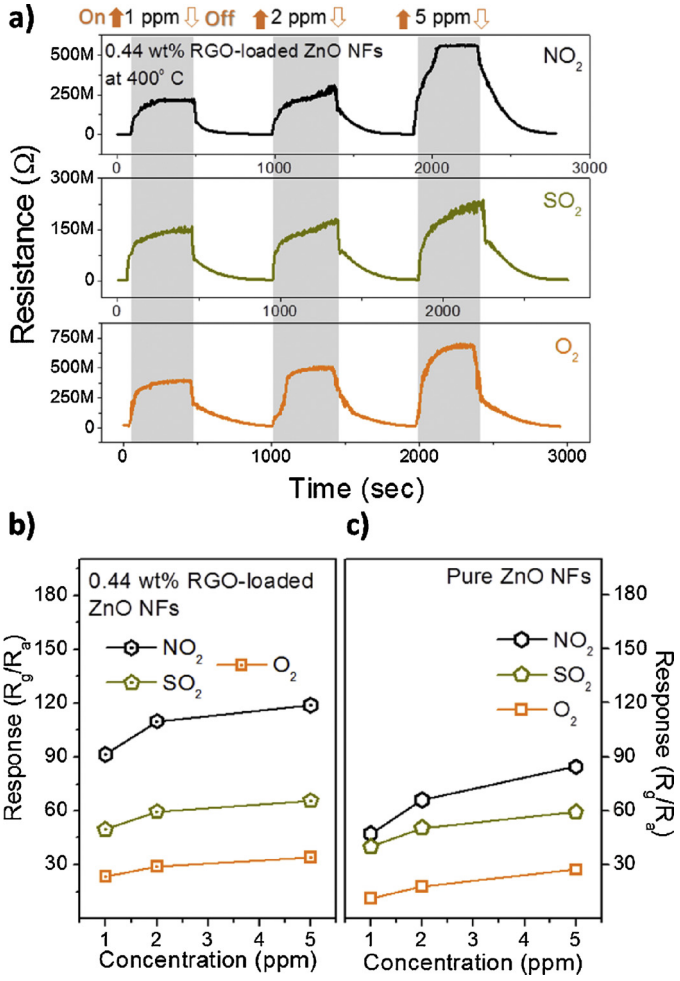

Fig. 4. (a) The dynamic sensing curves 0.44 wt% RGO-loaded ZnO NFs for oxidizing gases and (b) response of oxidizing gases as a function of gas concentration.

The sensor containing 0.44 wt% RGO NSs showed a higher response than the other sensors at all temperatures (Fig. 3a). The sensor response decreased once the amount of RGO NSs increased above 0.44 wt%, indicating that the amount of RGO NSs must be optimized in order to achieve the best sensing properties. The upper-right inset in Fig. 3b demonstrates the typical change in resistance of the sensors upon the supply and stoppage of NO_2 gas.

In order to further investigate the sensing properties, the responses of the sensors were measured against other oxidizing gases, such as SO_2 and O_2, at 400 °C. The dynamic sensing curves of oxidizing gases are shown in Fig. 4a. The data for the sensing responses are summarized in Fig. 4b. The responses to SO_2 and O_2 were significantly lower than the response to NO_2, which is mainly due to the higher reactivity of NO_2 gas molecules to general sensing materials as compared to SO_2 and O_2 [37]. For comparison, the responses of pure ZnO NFs to the oxidizing gases are shown in Fig. 4c. Fig. 4b and c and Table S1 clearly reveal that the loading of RGO NSs into ZnO NFs significantly enhances the sensitivity of the ZnO NFs. Close examination reveals that the incorporation of RGO NSs significantly enhanced the sensing response to NO_2 gas.

The sensor containing 0.44 wt% RGO NSs was further examined with different reducing gases (CO, C_6H_6, and C_2H_5OH). These dynamic sensing curves are shown in Fig. 5a, exhibiting typical *n*-type behavior. Upon introduction of the reducing gases, the resistivity of the sensors decreased and then again increased to the maximum level upon the removal of the gas. The sensing behavior of *n*-type semiconductors toward reducing analytes is exactly opposite to that of the oxidizing analytes and can be defined by the reduction–reoxidation mechanism [1]. The reducing gases react and partially reduce the oxide surface, leading to an increase in the number of free electrons in the conduction band (i.e., a reduced resistivity). Reoxidation of the surface occurs upon desorption or removal of the reducing analyte, leading to an increase in the conductivity. The responses of the reducing gases (and the results of pure ZnO NFs) are summarized in Fig. 5b and Table S2 as a function of gas concentration. Again, the responses of RGO-loaded ZnO NFs were superior relative to the pure ZnO NFs, clearly demonstrating the effectiveness of the RGO NSs. This improved performance may be caused by the formation of local heterojunctions at the RGO/ZnO interfaces.

In order to explain the operation of the sensing mechanisms in RGO-loaded ZnO NFs that leads to their exceptionally high sensitivity, several mechanisms must be considered. First, there is the modulation of the resistance along the surface of the ZnO NFs. In air ambient conditions, oxygen molecules adsorb, diffuse, and trap electrons from the surface of ZnO NFs to form atomic and molecular ions (O^-, O^{2-}, and O_2^-) [38]. An electron-depleted region is established within the Debye length underneath the surface due to the extraction of electrons by these adsorbed ions. The width of the depleted region increases or decreases as the chemisorbed oxygen reacts with the oxidizing or reducing analytes, respectively.

For example, the interaction of reducing analytes (e.g., C_2H_5OH, CO, and C_6H_6) has been proposed in the literature [1,35,39], as follows:

$$C_2H_5OH_{(g)} + O^-_{(ad)} \leftrightarrow CH_3CHO_{(g)} + H_2O_{(g)} + e^- \quad (1)$$

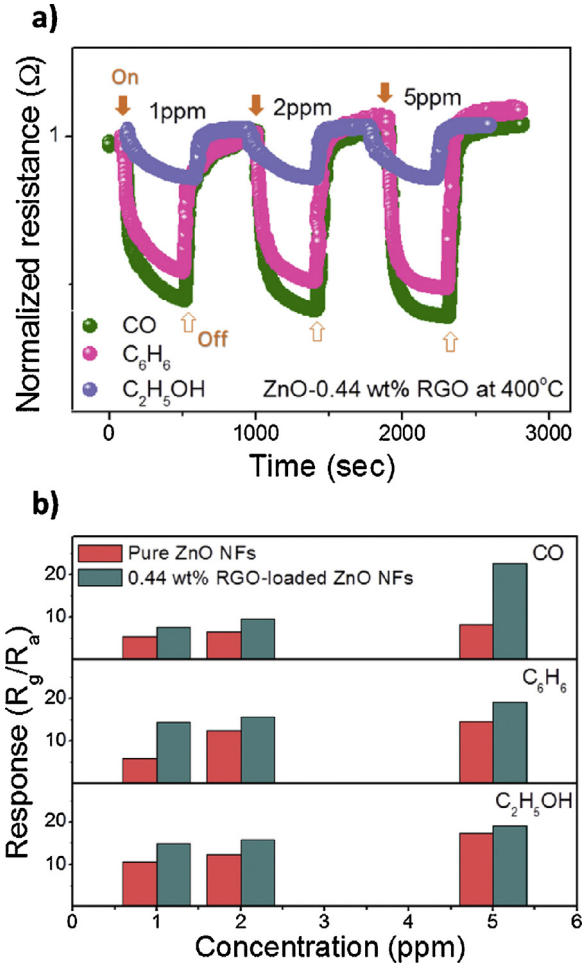

Fig. 5. (a) The dynamic sensing curves of 0.44 wt% RGO-loaded ZnO NFs for reducing gases and (b) comparison of the responses of 0.44 wt% RGO-loaded ZnO NFs with pure ZnO NFs for reducing gases.

$$CO_{(g)} + O^-_{(ad)} \leftrightarrow CO_{2(g)} + e^- \quad (2)$$

$$C_6H_{6(g)} + O^-_{(ad)} \leftrightarrow CO_{2(g)} + H_2O_{(g)} + 15e^- \quad (3)$$

Second, we will explain the sensing mechanism of monolithic ZnO NFs, in regard to the ZnO/ZnO homointerfaces (Fig. 6a). The gas sensing properties of NFs are mainly related to the presence of nanograins in the polycrystalline sensing materials. The boundaries between these nanograins act as potential barriers to the flow of electrons. In air ambient, the adsorbed oxygen (such as O^-) will be present at the grain boundaries of ZnO. The adsorbed species extract electrons by the reactions such as the following: $2O^- + V_{O^{\cdot\cdot}} + 2e^- \leftrightarrow O_O$ [40]. Accordingly, the potential barrier to the flow of electrons will appear at the boundaries. Upon the introduction of oxidizing and reducing gases, the potential barrier will become higher and lower, respectively, thereby increasing and decreasing the resistance across the grain boundaries along the ZnO NFs. The sensing enhancement with the ZnO/ZnO homointerfaces can also be explained by the evolution of the depletion layer along the grain boundaries. The resistance modulation arises from nanograin boundaries, by the expansion or suppression of the depletion layer.

Third, the RGO NSs-loaded ZnO NFs offer additional sources for sensor enhancement, being compared to the pure ZnO NFs. We will explain the sensing mechanism, with respect to the ZnO/RGO heterointerfaces (Fig. 6b). With a large amount of RGO NSs being distributed in the ZnO NFs, no direct contact will take place between the neighboring RGO NSs. Since the adjacent NSs are not physically connected, the electrical conduction in the sensor devices will mainly occur through the ZnO NFs, rather than discretely distributed RGO NSs. Fig. 6b indicates that a considerable amount of local heterojunctions (i.e. ZnO/RGO composite system) exists in RGO NS-loaded ZnO NFs.

It is possible that the ZnO/RGO interfaces as well as ZnO grain boundaries will contribute to the enhancement of sensing behavior. In the heterojunctions, the Fermi energy of ZnO is supposed to be lower than that of RGO, with the work functions of *n*-ZnO and RGO being about 5.20 and 4.75 eV, respectively (Fig. 6b). The RGO will be regarded as a kind of metal-like material. In order to equate the Fermi level, electrons will be transferred from RGO to *n*-ZnO. Resulting from the charge transfer, the potential barrier will be formed at heterojunctions, with the bending of the vacuum energy level and the energy band. In the present case, in which the work function of the metal is lower than that of the *n*-type semiconductor, the ohmic contact will be generated, becoming a non-rectifying barrier to the flow of electrons. In spite of the non-rectifying nature, the established potential barrier will affect the sensing behavior.

As a first possibility, the enlarged surface depletion region of ZnO NFs will enhance the sensing behavior. Since ZnO becomes more *n*-type than the original state, the energy barrier between ambient gas and ZnO will be further reduced [41,42], presumably enlarging the surface depletion region and thus reducing the conduction region simultaneously. With the increased initial resistance, the modulation of resistance by the sensing target gas will turn out to be a higher sensitivity (Text S1 in Supplementary material).

As a second possibility, the electrical current across the ZnO/RGO interfaces will provide additional modulation of resistance. In air ambient, the adsorbed oxygen will be present not only at the grain boundaries of ZnO, but also at the ZnO/RGO interfaces. The reducing gases will react with adsorbed oxygen such as O^-, providing electrons. The oxidizing gases will react with the adsorbed oxygen or provide the adsorbed oxygen, ultimately taking out electrons. The reducing and oxidizing gases will decrease and increase the height of the potential barriers to the electrons, respectively. In air ambient, the electron will easily flow from ZnO to RGO, because there is no potential barrier from ZnO to RGO (Fig. 6b). For electrical conduction through the sensor devices in terms of RGO NSs, the electrons, which were penetrated into the RGO, need to be taken out of the RGO NSs. However, the barrier height at the heterointerfaces (i.e. 4.5 eV) will prevent the electrons from escaping to the outer ZnO grains. Upon the introduction of oxidizing gas, the potential barrier will be enhanced at the *n*-ZnO/RGO interfaces, increasing the relative energy level of *n*-ZnO to RGO. Accordingly, the electron flow of RGO to *n*-ZnO will become much more difficult, ultimately increasing the resistance of the sensor. On the other hand, upon the introduction of reducing gas, the energy level of *n*-ZnO will be suppressed, reducing the relative energy level of *n*-ZnO to RGO. Accordingly, the electron flow of RGO to *n*-ZnO will become easier, ultimately decreasing the resistance of the sensor. The example of the NO_2 gas sensing is presented in Supplementary material (Text S2).

As a third possibility, discretely distributed RGO NSs, which are nanostructures with a higher surface accessibility [43], will exert the spillover effect, playing a catalytic role in adsorption, dissociation, and transportation (to neighboring ZnO surface) of NO_2 gas molecules. A lot of defects and functional groups on the RGO surface will provide adsorption sites for the gas molecules and will increase the sensitivity [41].

Although graphene oxide (GO) contains saturated sp^3 carbon atoms bound to oxygen, which makes it an insulator, reduced graphene oxide (RGO) still contains residual oxygen that is sp^3 bonded to the carbon atoms [44]. It is commonly accepted that the thermal annealing of GO or RGO will reduce the oxygen

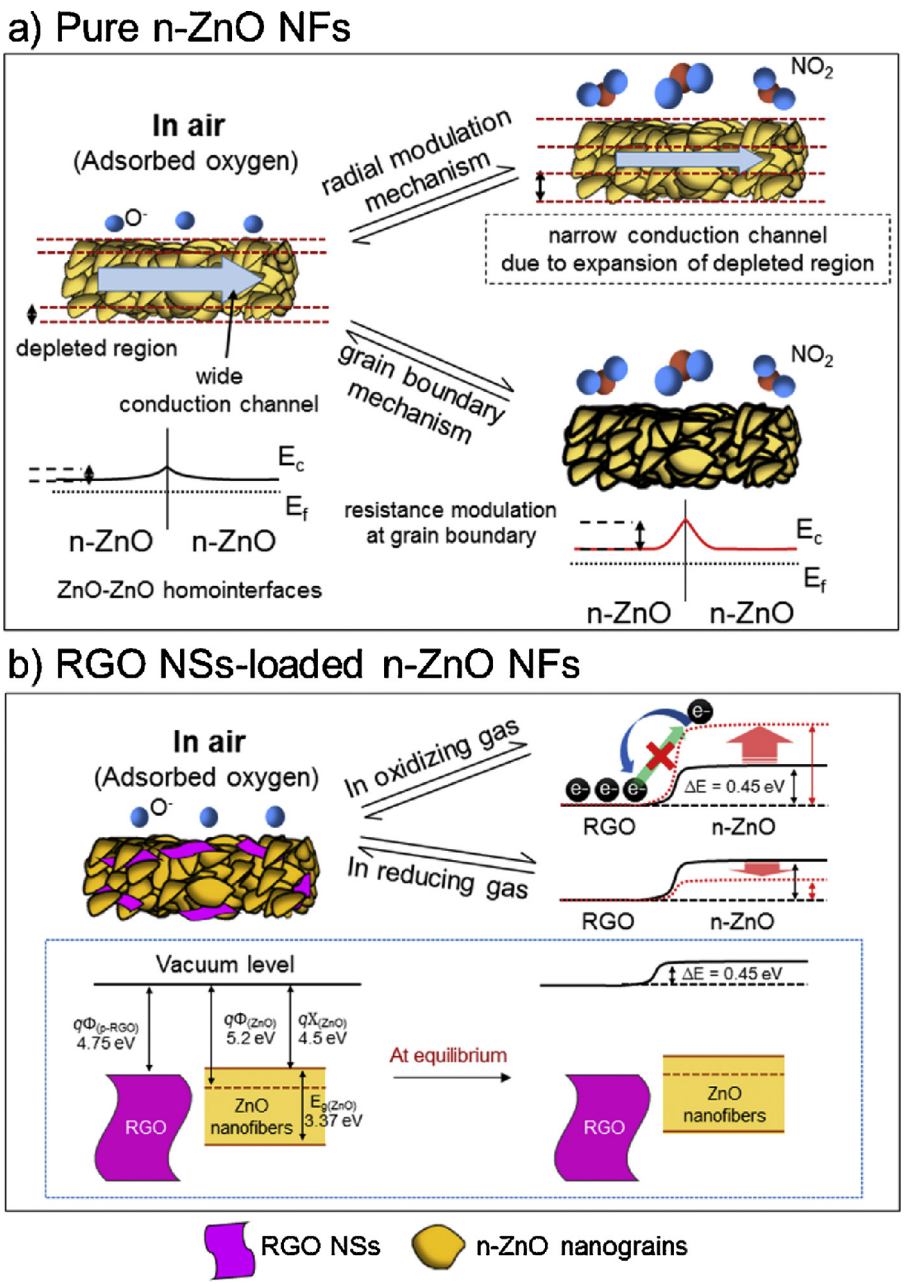

Fig. 6. Schematic illustration of sensing mechanism of (a) pure *n*-ZnO NFs and (b) RGO-ZnO heterojunctions.

functional groups. Accordingly, by the heating at 350–400 °C during the sensing tests, it is expected that the RGO embedded in ZnO nanofibers will be further reduced by losing oxygen. Since the currents in the sensing device mainly flow through continuous ZnO, the surface of RGOs, which is exposed to ambient, will play a catalytic role only.

Due to the resistance modulation caused by these sources, RGO-loaded *n*-ZnO NFs showed a larger change in their resistance compared to monolithic ZnO NFs. The resistance of the sensors increased upon the addition of RGO and reached a maximum at 0.44 wt%. At higher concentrations of RGO NSs, the resistance decreased. After this critical value, further additions of RGO NSs had no substantial effect on the resistance change of the sensors. However, at this time, we cannot explain why further loading of RGO NSs (above 0.44 wt%) unexpectedly decreases the sensing behavior. An additional systematic study is currently underway to describe this phenomenon in a following report.

Accordingly, we suggest that the combination of two sensing mechanisms, being related to ZnO/ZnO homointerfaces and RGO/ZnO heterointerfaces, is responsible for the enhancement of the sensing capabilities of RGO-loaded ZnO NFs. Thus, we can safely conclude that this hybrid sensing mechanism, which combines the effects of radial resistance modulation, ZnO/ZnO grain boundary modulation, and local heterojunctions (due to the presence of RGO NSs), is primarily responsible for the enhancement of the sensitivity of *n*-ZnO NFs.

Although the present sensor is comprised of RGO, this work focused mainly on the ZnO NFs sensors, because main conduction occurs through the continuous ZnO NFs, rather than discrete RGO NSs. The role of RGO NSs in enhancing the sensitivity is mainly related to the generation of ZnO/RGO heterojunctions and in addition, discrete RGO NFs will exert the spillover effect, playing a catalytic role in adsorption, dissociation, and transportation (to neighboring ZnO surface) of NO_2 gas molecules. Accordingly, direct

comparison between the present sensor and RGO or graphene-based sensors is meaningless. W. Yuan et al. summarized the sensing capabilities of graphene-based gas sensors [45]. Graphene sensor has a particularly different application, from the conventional semiconductor sensors, such as ZnO. Graphene has the lowest resistivity at room temperature among the substances and small amount of extra electrons can cause a noticeable change in the conductance of graphene. Accordingly, it will be suitable for low temperature and extremely low-concentration operation. As shown in Table 1 of Ref. [45], the actual sensitivity is relatively low, i.e. less than 2. It is noteworthy that the composite materials including graphene will attain the sensor responses higher than 2. For example, highly aligned SnO_2 nanorods on graphene nanosheets exhibited a sensor response of 2.1 for H_2S gas [46]. Also, vertically aligned ZnO nanorods and graphene hybrid structures exhibited a sensor response of 2.1 for ethanol gas [47]. However, in the present work, we embedded RGO NSs into ZnO NFs, assigning unusual roles to the RGO NSs and attaining the very high sensor response.

From Figs. 4 and 5 (Tables S1 and S2), we reveal that the sensor responses of RGO-loaded ZnO NFs to NO_2, SO_2, O_2, CO, C_6H_6, and C_2H_5OH are 119.0, 65.7, 34.2, 22.6, 19.1, and 19.1, respectively, at a gas concentration of 5 ppm. The RGO-loaded ZnO NFs turned out to become an excellent gas sensor for main oxidant and reductive gases. Further techniques including the functionalization will be necessary to enhance the sensor selectivity for a particular gas.

The response times of RGO-loaded ZnO NFs to NO_2 gases are 174, 350, and 143 s at 1, 2, and 5 ppm, respectively (Table S1). The recovery times of RGO-loaded ZnO NFs to NO_2 gases are 107, 188, and 259 s at 1, 2, and 5 ppm, respectively (Table S3). The initial resistances of RGO-loaded ZnO NFs to NO_2 gases are 3.39, 2.82, and 3.30 MΩ at 1, 2, and 5 ppm, respectively, exhibiting the stable sensing behavior (Table S4). In addition, the long-term stability of the RGO-loaded ZnO NFs was fine; after keeping in air ambient for 2 months, no noticeable sensing difference was observed. The long-term stability of the RGO-loaded ZnO NFs is presented in Fig. S4. After 6 months, the sensor responses to CO gas were decreased by 68.0, 72.1, and 39.8%, respectively, at CO concentrations of 1, 2 and 5 ppm. Further study will be necessary to improve the long-term stability of the present sensor.

4. Conclusion

We have successfully prepared RGO-loaded ZnO NFs by an electrospinning method. Microstructural investigation revealed that the addition of RGO NSs does not affect the size of the ZnO nanograins or NFs. The XRD spectrum of RGO-loaded ZnO NFs exhibits a very weak RGO (0 0 2) peak, as well as ZnO-related peaks. We have performed sensing tests with a variety of gases, including O_2, SO_2, NO_2, CO, C_6H_6, and C_2H_5OH, which show that our sensors exhibit excellent sensing capabilities. The sensor response to 5 ppm NO_2 gas was increased by the addition of RGO to ZnO NFs, reaching a maximum and optimal value of 150 at an RGO concentration of 0.44 wt% at 400 °C. Overall, the RGO-loaded ZnO NFs showed higher sensitivity to different oxidizing and reducing gases compared to monolithic ZnO NFs. We ascribed this improvement in performance to the hybrid sensing mechanism, which combines the effects of the surface depletion layer of ZnO NFs (radial resistance modulation), potential barriers at ZnO grain boundaries (ZnO/ZnO homointerfaces), and RGO-NSs/ZnO heterointerfaces.

Due to the work function difference of RGO and ZnO, the potential barrier will be generated at the heterointerfaces. This novel hybrid sensing mechanism is responsible for the outstanding sensitivity of RGO-loaded ZnO NFs.

Acknowledgements

This work was supported by a National Research Foundation of Korea (NRF) grant funded by the Ministry of Education, Science and Technology (MEST) of Korea (no. 2012R1A2A2A01013899), and the International Research & Development Program of NRF funded by MEST (no. 2013K1A3A1A21000149).

Appendix A. Supplementary data

Supplementary data associated with this article can be found, in the online version, at http://dx.doi.org/10.1016/j.snb.2015.07.120

References

[1] A. Tricoli, M. Righettoni, A. Teleki, Semiconductor gas sensors: dry synthesis and application, Angew. Chem. Int. Ed. Engl. 49 (2010) 7632–7659.
[2] M.M. Arafat, B. Dinan, S.A. Akbar, A.S. Haseeb, Gas sensors based on one dimensional nanostructured metal-oxides: a review, Sensors 12 (2012) 7207–7258.
[3] Z. Li, H. Zhang, W. Zheng, W. Wang, H. Huang, C. Wang, et al., Highly sensitive and stable humidity nanosensors based on LiCl doped TiO_2 electrospun nanofibers, J. Am. Chem. Soc. 130 (2008) 5036–5037.
[4] Z.-M. Huang, Y.-Z. Zhang, M. Kotaki, S. Ramakrishna, A review on polymer nanofibers by electrospinning and their applications in nanocomposites, Compos. Sci. Technol. 63 (2003) 2223–2253.
[5] Y. Zhang, X. He, J. Li, Z. Miao, F. Huang, Fabrication and ethanol-sensing properties of micro gas sensor based on electrospun SnO_2 nanofibers, Sens. Actuators B: Chem. 132 (2008) 67–73.
[6] Z. Zhang, X. Li, C. Wang, L. Wei, Y. Liu, C. Shao, ZnO hollow nanofibers: fabrication from facile single capillary electrospinning and applications in gas sensors, J. Phys. Chem. C 113 (2009) 19397–19403.
[7] G. Wang, Y. Ji, X. Huang, X. Yang, P.-I. Gouma, M. Dudley, Fabrication and characterization of polycrystalline WO_3 nanofibers and their application for ammonia sensing, J. Phys. Chem. B 110 (2006) 23777–23782.
[8] D.-J. Yang, I. Kamienchick, D.Y. Youn, A. Rothschild, I.-D. Kim, Ultrasensitive and highly selective gas sensors based on electrospun SnO_2 nanofibers modified by Pd loading, Adv. Funct. Mater. 20 (2010) 4264–4528.
[9] W.E. Teo, S. Ramakrishna, A review on electrospinning design and nanofiber assemblies, Nanotechnology 17 (2006) R89–R106.
[10] S.-W. Choi, J.Y. Park, S.S. Kim, Synthesis of SnO_2–ZnO core–shell nanofibers via a novel two-step process and their gas sensing properties, Nanotechnology 20 (2009) 465603.
[11] I.D. Kim, A. Rothschild, B.H. Lee, D.Y. Kim, S.M. Jo, H.L. Tuller, Ultrasensitive chemiresistors based on electrospun TiO_2 nanofibers, Nano Lett. 6 (2006) 2009–2013.
[12] J.-W. Yoon, J.-K. Choi, J.-H. Lee, Design of a highly sensitive and selective C_2H_5OH sensor using p-type Co_3O_4 nanofibers, Sens. Actuators B 161 (2012) 570–577.
[13] X. Wang, C. Drew, S.-H. Lee, K.J. Senecal, J. Kumar, L.A. Samuelson, Electrospun nanofibrous membranes for highly sensitive optical sensors, Nano Lett. 2 (2002) 1273–1275.
[14] B. Ding, M. Wang, J. Yu, G. Sun, Gas sensors based on electrospun nanofibers, Sensors 9 (2009) 1609–1624.
[15] C. Lee, S.W. Choi, J.Y. Park, S.S. Kim, Synthesis of ZnO nanofibers and their gas sensing properties, Sensor Lett. 9 (2011) 132–136.
[16] S.-H. Choi, G. Ankonina, D.Y. Youn, S.-G. Oh, J.-M. Hong, A. Rothschild, et al., Hollow ZnO nanofibers fabricated using electrospun polymer templates and their electronic transport properties, ACS Nano 3 (2009) 2623–2631.
[17] M. Ahmad, C. Pan, Z. Luo, J. Zhu, A single ZnO nanofiber-based highly sensitive amperometric glucose biosensor, J. Phys. Chem. C 114 (2010) 9308–9313.
[18] L. Liu, S. Li, J. Zhuang, L. Wang, J. Zhang, H. Li, et al., Improved selective acetone sensing properties of Co-doped ZnO nanofibers by electrospinning, Sens. Actuators B: Chem. 155 (2011) 782–788.
[19] L. Wang, S. Wang, M. Xu, X. Hu, H. Zhang, Y. Wang, et al., A Au-functionalized ZnO nanowire gas sensor for detection of benzene and toluene, Phys. Chem. Chem. Phys. 15 (2013) 17179–17186.
[20] Y. Zheng, L. Zheng, Y. Zhan, X. Lin, Q. Zheng, K. Wei, Ag/ZnO heterostructure nanocrystals: synthesis, characterization, and photocatalysis, Inorg. Chem. 46 (2007) 6980–6986.
[21] N. Tamaekong, C. Liewhiran, A. Wisitsoraat, S. Phanichphant, Sensing characteristics of flame-spray-made Pt/ZnO thick films as H_2 gas sensor, Sensors 9 (2009) 6652–6669.
[22] S.M. Wang, P. Wang, Z.F. Li, C.H. Xiao, B.X. Xiao, R. Zhao, et al., Highly enhanced methanol gas sensing properties by $Pd_{0.5}Pd_3O_4$ nanoparticle loaded ZnO hierarchical structures, RSC Adv. 4 (2014) 35375–35382.
[23] Z. Ling, C. Leach, R. Freer, Heterojunction gas sensors for environmental NO_2 and CO_2 monitoring, J. Eur. Ceram. Soc. 21 (2001) 1977–1980.
[24] Y. Hu, X. Zhou, Q. Han, Q. Cao, Y. Huang, Sensing properties of CuO–ZnO heterojunction gas sensors, Mater. Sci. Eng. B 99 (2003) 41–43.

[25] G. Lu, S. Park, K. Yu, R.S. Ruoff, L.E. Ocola, D. Rosenmann, et al., Toward practical gas sensing with highly reduced graphene oxide: a new signal processing method to circumvent run-to-run and device-to-device variations, ACS Nano 5 (2011) 1154–1164.
[26] L.H. Tang, Y. Wang, Y.M. Li, H.B. Feng, J. Lu, J.H. Li, Preparation, structure, and electrochemical properties of reduced graphene sheet films, Adv. Funct. Mater. 19 (2009) 2782–2789.
[27] E. Llobet, Gas sensors using carbon nanomaterials: a review, Sens. Actuators B: Chem. 179 (2013) 32–45.
[28] F. Schedin, A.K. Geim, S.V. Morozov, E.W. Hill, P. Blake, M.I. Katsnelson, et al., Detection of individual gas molecules adsorbed on graphene, Nat. Mater. 6 (2007) 652–655.
[29] W. Yuan, G. Shi, Graphene-based gas sensors, J. Mater. Chem. A 1 (2013) 10078–10091.
[30] A.S.M.I. Uddin, G.S. Chung, Synthesis of highly dispersed ZnO nanoparticles on graphene surface and their acetylene sensing properties, Sens. Actuators B: Chem. 205 (2014) 338–344.
[31] T.V. Khai, H.G. Na, D.S. Kwak, Y.J. Kown, H. Ham, K.B. Shim, H.W. Kim, Significant enhancement of blue emission and electrical conductivity of N-doped graphene, J. Mater. Chem. 22 (2012) 17992–18003.
[32] A. Katoch, G.J. Sun, S.W. Choi, J.H. Byun, S.S. Kim, Competitive influence of grain size and crystallinity on gas sensing performances of ZnO nanofibers, Sens. Actuators B: Chem. 185 (2013) 411–416.
[33] S. Stankovich, D.A. Dikin, R.D. Piner, K.A. Kohlhaas, A. Kleinhammes, Y. Jia, et al., Synthesis of graphene-based nanosheets via chemical reduction of exfoliated graphite oxide, Carbon 45 (2007) 1558–1565.
[34] P. Cui, J. Lee, E. Hwang, H. Lee, One-pot reduction of graphene oxide at subzero temperatures, Chem. Commun. 47 (2011) 12370–12372.
[35] H.W. Kim, M.A. Kebede, H.S. Kim, B. Srinivasa, D.Y. Kim, J.Y. Park, et al., Effect of growth temperature on the ZnO nanowires prepared by thermal heating of Zn powders, Curr. Appl. Phys. 10 (2010) 52–56.
[36] J. Zhang, H. Yang, G. Shen, P. Cheng, J. Zhang, S. Guo, Reduction of graphene oxide via L-ascorbic acid, Chem. Commun. 46 (2010) 1112–1114.
[37] M. Chen, Z.H. Wang, D.M. Han, F.B. Gu, G.S. Guo, Porous ZnO polygonal nanoflakes: synthesis, use in high-sensitivity NO_2 gas sensor, and proposed mechanism of gas sensing, J. Phys. Chem. C 115 (2011) 12763–12773.
[38] N. Barsan, U. Weimar, Conduction model of metal oxide gas sensors, J. Electroceram. 7 (2001) 143–167.
[39] V.S. Vaishnav, S.G. Patel, J.N. Panchal, Development of ITO thin film sensor for detection of benzene, Sens. Actuators B 206 (2015) 381–388.
[40] S.S. Kim, J.Y. Park, S.-W. Choi, H.G. Na, J.C. Yang, H.W. Kim, Enhanced NO_2 sensing characteristics of Pd-functionalized networked In_2O_3 nanowires, J. Alloys Compd. 509 (2011) 9171–9177.
[41] K. Anand, O. Singh, M.P. Singh, J. Kaur, R.C. Singh, Hydrogen sensor based on graphene/ZnO nanocomposite, Sens. Actuators B 195 (2014) 409–415.
[42] R. Zou, G. He, K. Xu, Q. Liu, Z. Zhang, J. Hu, ZnO nanorods on reduced graphene sheets with excellent field emission, gas sensor and photocatalytic properties, J. Mater. Chem. A 1 (2013) 8445–8452.
[43] Q. Lin, Y. Li, M. Yang, Tin oxide/graphene composite fabricated via a hydrothermal method for gas sensors working at room temperature, Sens. Actuators B 173 (2012) 138–147.
[44] A. Bagri, C. Mattevi, M. Acik, Y.J. Chabal, M. Chhowalla, V.B. Shenoy, Structural evolution during the reduction of chemically derived graphene oxide, Nat. Chem. 2 (2010) 581–587.
[45] W. Yuan, G. Shi, Graphene-based gas sensors, J. Mater. Chem. A 1 (2013) 10091–19978.
[46] Z. Zhang, R. Zou, G. Song, L. Yu, Z. Chen, J. Hu, Highly aligned SnO_2 nanorods on graphene sheets for gas sensors, J. Mater. Chem. 21 (2011) 17360–17365.
[47] J. Yi, J.M. Lee, W.I. Park, Vertically aligned ZnO nanorods and graphene architectures for high-sensitive flexible gas sensors, Sens. Actuators B 155 (2011) 264–269.

Biographies

Zain Ul Abideen received his B.S. (Engineering) degree in materials science and engineering from Ghulam Ishaq Khan Institute of Engineering Sciences and Technology (GIKI), Pakistan in June 2014. He is presently a graduate student pursuing his research at Inha University, South Korea under the supervision of Professor Sang Sub Kim since September 2014. His research interests include synthesis of composite nanomaterials, metal oxide based semiconductors and their applications in chemical sensors.

Akash Katoch received his B.S. degree from Himachal Pradesh University, India in 2004. In 2006, he received his M.S. degree in applied physics from Kurukshetra University, Kurukshetra, India. He received his M.Tech. degree in Material Science & Engineering from Thapar University, India, in 2009. In 2014, he received his Doctoral degree from Inha University, Republic of Korea. From 2014 onwards he has been a postdoctoral fellow at Inha University, Republic of Korea. He has been working on metal oxide gas sensors synthesized by the sol–gel process, electrospinning and VLS method.

Jae-Hun Kim received his B.S. degree from Gyeongsang National University, Republic of Korea in 2013. In February 2015, he received an M.S. degree from Inha University, Republic of Korea. He is now working as a Ph.D. candidate at Inha University, Republic of Korea. He has been working on oxide nanowire gas sensors.

Yong Jung Kwon received his B.Eng. degree in materials science and engineering from Hanyang University, Korea in 2012. He is currently a graduate student in Hanyang University. His research work is to focus on nanomaterials and their application to gas sensors.

Hyoun Woo Kim joined the Division of Materials Science and Engineering at Hanyang University as a full professor in 2011. He received his B.S. and M. S. degrees from Seoul National University and his Ph.D. degree from Massachusetts Institute of Technology (MIT) in electronic materials in 1986, 1988, and 1994, respectively. He was a senior researcher in the Samsung Electronics Co., Ltd. from 1994 to 2000. He has been a professor of materials science and engineering at Inha University from 2000 to 2010. He was a visiting professor at the Department of Chemistry of the Michigan State University, in 2009. His research interests include the one-dimensional nanostructures, nanosheets, and gas sensors.

Sang Sub Kim joined the Department of Materials Science and Engineering, Inha University, in 2007 as a full professor. He received his B.S. degree from Seoul National University and his M.S and Ph.D. degrees from Pohang University of Science and Technology (POSTECH) in Material Science and Engineering in 1987, 1990, and 1994, respectively. He was a visiting researcher at the National Research in Inorganic Materials (currently NIMS), Japan for 2 years each in 1995 and in 2000. In 2006, he was a visiting professor at Department of Chemistry, University of Alberta, Canada. In 2010, he also served as a cooperative professor at Nagaoka University of Technology, Japan. His research interests include the synthesis and applications of nanomaterials such as nanowires and nanofibers, functional thin films, and surface and interfacial characterizations.